Conic optical fiber probe for generation and characterization of microbubbles in liquids.

J. E. Muñoz-Pérez[1], J. L. Cruz[2*], M.V. Andrés[2], J. G. Ortega-Mendoza[1]

[1] División Posgrado, Universidad Politécnica de Tulancingo, Calle Ingenierías No. 100, Huapalcalco, Tulancingo, Hidalgo, 43629, México.
[2] Departamento de Física Aplicada y Electromagnetismo-ICMUV, Universidad de Valencia, Dr. Moliner 50. Burjassot, 46100, España.

*Corresponding author
E-mail address: cruz@uv.es

Received xxxxxx
Accepted xxxxxx
Available online xxxxxx

Abstract

A novel optical fiber probe has been developed to provide mechanical stability to microbubbles generated in fluids, the tip of the fiber is etched with hydrofluoric acid to pierce a truncated horn that fastens the microbubbles to the fiber tip and prevents misalignment or detachment caused by convection currents, vibrations or shocks in the liquid. Microbubbles are photo-thermally generated on the etched fiber and used as Fabry-Perot cavity sensor. Two methods were used to interrogate the probe: the first one, in the wavelength domain, is suitable for calibration in static or quasi static situations; the second one, in the time domain, can be used in dynamic environments. Experimental results in the wavelength domain show that the microbubble size rises linearly with temperature and decreases with the inverse of pressure; the average slopes are 27.1 μm/^{0}C and 88.3 μm/bar respectively. Dynamic variations of temperature have been measured in the time domain, temperature changes down to 0.007 ^{0}C have been detected at a readout rate of 10 s^{-1}. Bubbles have been subjected to pressure shocks of 2.4 bar at a speed of 25 bar/s, pressure changes of 3.4 mbar have been resolved in the time domain at a readout rate of 20000 s^{-1}.

Keywords: Microfluidics; Microbubble; Optical fiber; Interferometry.

1. Introduction

A general objective of science and technology is the reduction in size, number of components and production costs of measurement systems. Optics takes great relevance in microfluidics since it offers new methods for matter manipulation [1, 2] and for the characterization of thermodynamic and mechanical properties of fluids [3], which leads to smaller optical devices with low or nil operating voltages, no moving mechanical parts, additional functionality and great potential in performance. Optical fibers are used in fluidics because of their small size, high sensitivity, and remote sensing capabilities [4]; furthermore, fibers are well suited to develop lab-onchip devices [5, 6]. Fabry-Perot interferometers (FPI) in optical fiber technology are widely used as interrogation instruments [7, 8] because they have high sensitivity to small changes in the environmental conditions and provide great precision when measuring physical variables such as temperature, pressure, voltage, magnetic field, flow rate, pH or refractive index, among others.

Acoustic interaction with microbubbles has a high potential for biosensing [9], vapor-based devices are being used for flow control [10] and microbubbles on optical fibers have been proposed as integrated flow regulators [11]. Microbubbles are generated by focused lasers [1, 12] or by optical fibers [2, 11, 13] and have been recently proposed to study the state and properties of the fluid.

The operation of this type of optofluidic devices is very different from traditional fiber optic sensors. It consists in a

https://doi.org/xx.xxxx/j.sna.xxxx.xx.xxxx xxxx-xxxx/

hybrid structure (solid / liquid / gas) generated by heating the tip of the fiber by the guided light and it can be regenerated with low cost and good performance. The thermal effect is achieved by absorption of light in micro or nanoparticles deposited on the fiber tip; gold, silver or zinc have been used as absorbers [2, 11, 14-15], the absorber is usually heated at a pump wavelength of 980 nm [11, 13]. The heat evaporates spherical bubbles which undergo deformations due to physical or chemical phenomena produced in the liquid where they are formed, these deformations are detected a probe laser at a typical wavelength of 1550 nm. The detection of small deformations of the microbubble has different applications in the study of physical, chemical or cellular phenomena [9-13].

Major drawbacks of this technique are the mechanical instability of the bubbles and the risk of detachment from the fiber tip when they are subjected to turbulences vibrations or shocks. Conic fiber tips have been used to fasten solid microlenses on fibers [16]. In this work we report on the fabrication of conical fiber probes for stabilization of microbubbles in liquids, the potential of the probe is demonstrated measuring pressure shocks. The concave cones are fabricated by etching the fiber tip, bubbles photothermally generated are trapped by the cone by a combination of adhesive forces, surface tension forces and viscosity forces; bubbles are held in place even when the diameter of the bubble is larger than the size of the cone. The bubbles diameters are measured interferometrically, both in the wavelength domain and in the time domain. The response of the bubbles to temperature or pressure variations is characterized by static measurements in the wavelength domain; calibration curves reveal that the bubbles diameter increases linearly with temperature and decreases with the inverse of pressure in the ranges under test. Dynamic changes have been detected in the time domain, temperature variations in short intervals of time or pressure shocks have been optically measured as function of time from the static calibrations.

2. Material and Methods

A Fabry-Perot interferometer is formed by two opposite interfaces of the bubble acting as semi-transparent mirrors in front of the optical fiber, a diagram is shown in Fig. 1 (top). It can be considered that the interfering rays are those travelling parallel to the fiber axis, this is reasonable assumption for single mode fibers with core diameters of about 8 microns and numerical apertures of about 0.14; under this condition, the maxima of the interference signal occur when the phase difference of the interfering waves satisfies:

$$2\frac{2\pi n l}{\lambda} = m2\pi \qquad (1)$$

where l is the cavity length, n the refractive index of the gas, λ the operation wavelength and m an integer number. Working at constant wavelength and refractive index, the length increment corresponding to two consecutive interference fringes is given from (1) as:

$$\Delta l = l_{m+1} - l_m = \frac{\lambda}{2n} \qquad (2)$$

Working with fixed cavity length and refractive index, the wavelength difference between two consecutive fringes (free spectral range -FSR-) can be derived from (1) as:

$$FSR = \lambda_m - \lambda_{m+1} = \frac{\lambda_m \lambda_{m+1}}{2n\,l} \qquad (3)$$

The cavity length (or the refractive index) can be obtained from (3) when measurements are performed in the wavelength domain. Fast variations of the cavity length can be obtained from (2) when measuring as a function of time. Apart from these two reflections there is an additional reflection in the interface between the fiber glass and the liquid filling the dent, the power reflected by this interface is smaller than the power reflected by the surface of the bubble. For example, if the liquid is water with refractive index 1.33, the bubble is water vapor with an index close to 1 and the fiber has an effective index of about 1.45, the fraction of power reflected by the water-vapor interface is about 3.4% while the power reflected by the glass-water interface is about 0.19% (13 dB lower); therefore the wave reflected by fiber-water surface has only a minor effect on the main interference produced by the opposite sides of the bubble. For the dimensions of the probes and bubbles used in these experiments, the interference with the wave reflected by closest side of the bubble produces a large spectral period perturbation of the main interference pattern, while the interference with the wave reflected by the farthest surface produces a short period perturbation to the main interference, both perturbations increase the uncertainty of measurements unless they are filtered.

A conic hole was made in the tip of a single-mode optical fiber by introducing the fiber in a solution 25 wt.% hydrofluoric acid and 75 wt.% deionized water for 15 min. We used the DC1500 (11/125) 0.12HD fiber manufactured by Fibercore Ltd because it has phosphorus co-doped silica glass in the inner cladding which can be etched faster than the outer part of the cladding. The fiber has a numerical aperture of 0.12, a nominal core diameter of 6 μm and a cladding diameter 125 μm. The etching process shapes the fiber tip into a truncated conic horn as it can be seen in Fig. 2. The size of the cone depends directly on the time that the optical fiber is submerged in the acid solution, we have found that cones 25 μm wide and 20 μm deep are suitable for this application.

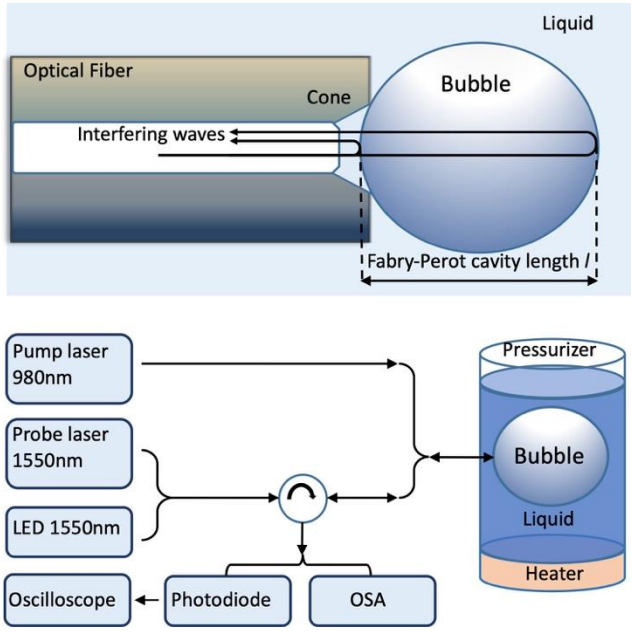

Figure 1. Diagram of the interaction of light in a microbubble (top). Scheme of the experimental setup for bubbles growth and characterization (bottom).

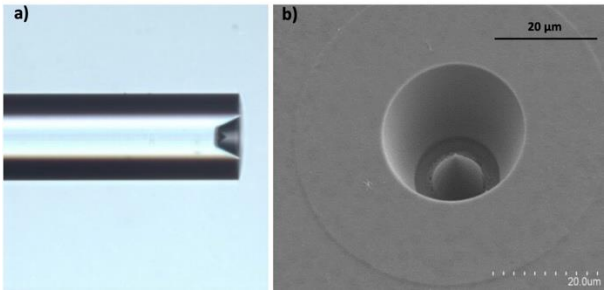

Figure 2. Micrographs of the cone formation on the fiber tip. Side view the of fiber taken with an optical microscope (a), front view of the fiber taken by a scanning electron microscope (b).

The incorporation of nanoparticles on the surfaces of the etched cone was carried out using the technique known as photodeposition [2,11,14]. Toner micro particles were used in the experiment, the particles without dissolving have a size between 3 and 30 μm, after being dissolved their sizes range between 70 and 700 nm [17]. We employed black toner provided by Ricoh (product code C3503) whose chemical composition according to the safety data sheet (MSDS number 841817) is a mixture of polyester resin (60-90 %), wax (1-20 %), carbon black (1-20 %), silica (<10 %) and titan oxide (0.1-1 %).The fiber tip was immersed in suspension of toner in water having 30 mgr of toner per 1.5 ml of water, after few seconds the particles stick on the fiber which is taken out of the suspension and dried. After the fiber has been coated with the particles it is immersed in a cell containing water, the bubbles are then generated at the tip of the conical fiber by heating the coating with a pump laser emitting at 980 nm as it is illustrated in Fig. 1 (bottom), the laser is coupled to the fiber cone through a WDM. When the pump laser is turned on, the nanoparticles absorb energy and evaporate water generating a microbubble on the fiber tip. It takes about 3 s to growth a bubble under a pump power of 116 mW, the bubble growth is visualized by a microscope objective and a camera. Once the bubble has the desired size the pump is turned off; it has been demonstrated in [18] that the lifetime of the bubbles depends on the square of the initial diameter and is dependent on the fluid as well, we found in our experiments that bubbles with diameters over 100 μm remain stable for tens of minutes, the presence of tonner particles in the surface of the bubbles probably contribute to enhance the stability. Some probes have been used several times to generate bubbles repeatedly, the growth of the bubbles does not suggest a significant reabsorption of the tonner layer by the liquid, this indicates that the deposition process (immersion, drying and first-time heating) provides sufficient adherence between the coating layer and the glass.

There is a number of mechanisms that contribute to trap the bubble on the fiber and to enhance the stability in comparison with a plat terminated prove. First, the bubble and the cone are in contact along a circular line (there is a single contact point in the case of a flat probe), this increases the effect of adhesive forces to the molecules to the glass. Second, while the bubble is growing there is a gradient of temperature in the surface of the bubble caused by the hot spot, this gradient causes a variation of surface tension which produces a force (Marangoni's force [2]) that pulls the bubble toward the vertex of the cone. Third, when the bubble is growing, there is a relative movement between the front surface of the bubble and the surrounding liquid, as a consequence a viscous force appears that drags the bubble toward the cone vertex guided by walls of the cone. Fourth and last, if a perturbation exerts a transverse force on the bubble, the bubble is deformed by compression against the wall of the cone, then, a restoring force appears that recovers the spherical shape of the bubble minimizing the energy associated to surface tension.

The diameter of the bubbles is measured in the wavelength domain, a LED was used as broad band light source and the interferometric fringes were measured with an optical spectrum analyzer (Yokogawa AQ6370C) as it can be seen in Fig. 1 (bottom). The light was launched into the fiber probe through a circulator and a WDM. Because the sweep time of the spectrum analyzer is of the order of one second this procedure is well suited to static situations (steady temperature, pressure or chemical composition).

Fast variations of the diameter are measured in the time domain detecting the interferometer output with a photodetector and an oscilloscope (Newport New Focus-2011 and AGILENT MS09104A) which are connected to the sensor head through a circulator and a WDM as it is indicated in Fig. 1. In this case the interferometer is fed with a laser diode emitting at 1550 nm and having a coherence length much larger than the Fabry-Perot cavity length; in both cases the optical power for monitorization is about 1mW, this is a hundred times smaller than the power used to generate the bubble.

3. Results and Discussion

We show first the benefit of using conic fibers tips instead of flat terminated fibers. Fig. 3 shows microbubbles generated at the tip of optical fibers with flat and with conic terminations. Fig. 3 (a) and (b) correspond to microbubbles on a flat optical probe subjected to pressures of 1 bar and 2 bar respectively. Fig. 3 (c) and (d) correspond to microbubbles in a cone-terminated fiber tip subjected to pressures of 1 and 3.5 bar, respectively; the cones are not visible in these pictures because they are partially filled of water and offer little contrast.

It can be seen that the bubbles on the etched fibers are well aligned with the fiber axis, even for big bubbles compared with the fiber diameter (Fig. 3 (c)). Furthermore, the fiber stays in the right position when the pressure suddenly rises (figure 3 (d)). On the contrary, the bubble on the flat terminated fiber has an eccentric position and it moves when the pressure changes. It is important to comment that the cone-terminated fiber improves the sphericity of the bubble as well.

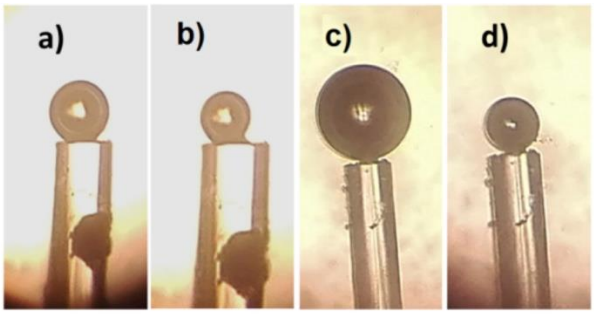

Figure 3. Microbubbles generated on optical fibers with flat termination (a and b) and with a conic termination (c and d) when subjecting the liquid to a pressure of 1 bar (a and c), 2 bar (b) and 3.5 bar (d).

The fiber diameter can be measured with higher accuracy as a consequence of the improved stability of the bubble on the cone. As an example, the diameters of two microbubbles growth in flat and in conic fibers were repeatedly measured at intervals of one minute, measurements were made at constant pressure and temperature. Fig. 4 shows the diameters measured in both cases, the diameters measured with the flat fiber have a dispersion of ±12 µm, while the diameters measured in the etched fiber have a dispersion of ±3 µm giving an accuracy of 1.5%. The major sources of dispersion in the first case are the vibrations of the system and convection currents in the liquid, in the second case the mechanical distortions have less effect while the ripples of the optical spectrum gain weight.

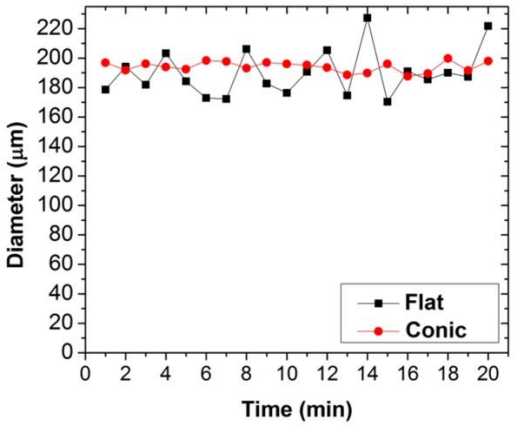

Figure 4. Diameter of two bubbles measured repeatedly by a flat probe and by a conic probe.

The microbubbles were calibrated in temperature and pressure from measurements in the wavelength domain. Fig. 5 shows the optical spectrum obtained width two different bubble sizes. The diameters are obtained from the distance between consecutive fringes and equation (3), the spectra of Fig. 5 (a) and (b) result in diameters of 96 µm and 238 µm respectively. The shortest measurable diameter is limited by the 30 nm bandwidth of the light source used in this experiment, then the FRS must be smaller than 15 nm to achieve good accuracy (diameters larger than 75 µm).

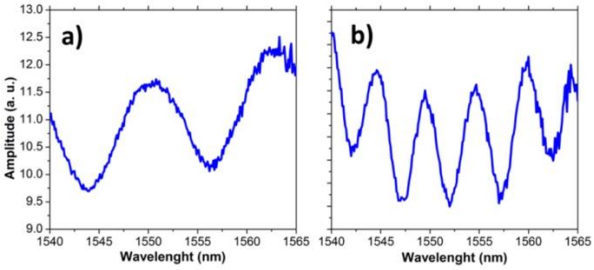

Figure 5. Optical spectra obtained with microbubbles of diameters: 96 µm (a), 238 µm (b).

The results of the thermal calibration at atmospheric pressure are shown in Fig. 6, this graph shows the FRS of the

optical spectra and the bubble diameter calculated from the FSR as a function of temperature. The measurements where preformed at a set of discrete temperatures, the temperature stability was better than ±0.1 ^{0}C during the time that takes to acquire the corresponding optical spectrum. The temperature was measured placing a thermocouple inside the water cell at a distance of about 1mm of the bubble, the bubble and the thermometer had symmetric positions with respect to the axis of the cell and were equidistant from the walls so that the thermometer reading is representative of the bubble temperature. One can observe that the FSR decreases with the inverse of temperature and that the corresponding bubble diameter presents a linear increase. The fitting expressions obtained from data are shown in the insets of Fig. 6, the experimental results show that the bubble diameter has a thermal sensitivity of 27.1 μm/^{0}C at atmospheric pressure in the range of diameters under test. The surface tension of water varies from 0.069 N/m to 0.067 N/m in this range of temperatures [19]; for an outer pressure of 1.013 bar, it is calculated that the pressure inside the bubble decreases from 1.035 to 1.018 bar when temperature rises.

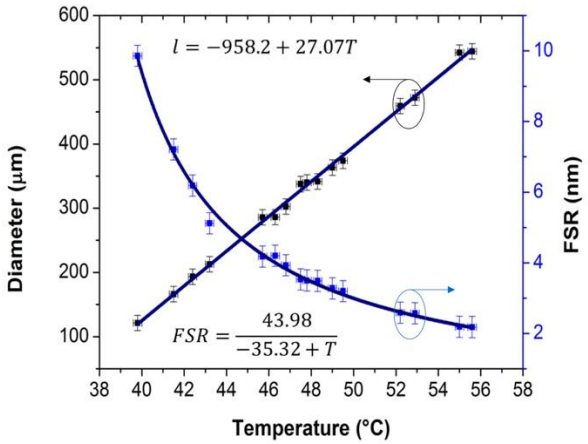

Figure 6. Bubble diameter and FSR as a function of temperature at atmospheric pressure.

Pressure calibration was performed with a bubble of approximately 460 μm on the tip of the fiber at a constant temperature of 24 ^{0}C, the bubble was growth with an overpressure 0.1 bar in a sealed cell. Fig. 7 shows the measured FSR as a function of pressure as well as the bubble diameter calculated from equation (3). It can be observed that the FSR increases linearly while the diameter of the bubble decreases with the inverse of pressure. The fitting expressions of the measured data are shown in the insets of the figure. The FSR has a sensitivity of 2.38 nm/bar, the diameter has a variable sensitivity ranging between 530 μm/bar at 1 bar and 14.7 μm/bar at 6 bar, being the full range average of 88.3 μm/bar. For a surface tension of 0.072 [19], the pressure inside the bubble varies between 1.05 bar and 6.33 bar when the external pressure increases from 1 to 6 bar.

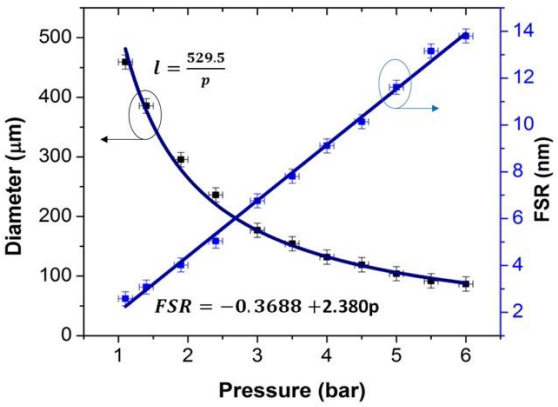

Figure 7. Bubble diameter and FSR as a function of pressure at room temperature.

The above calibrations have been carried out with bubbles growth to specific initial diameters, other bubbles would experience different variations with temperature or pressure depending on their initial diameter (the diameter when the bubble is growth), therefore, the calibration equations of figures 6 and 7 must be generalized by shifting the horizontal axis to the initial diameter of the bubbles as follows:

$$\boldsymbol{l = l_0 + 27.08(T - T_0)} \quad \textbf{(4)}$$

$$\boldsymbol{l = \frac{529.5}{p - p_0 + \frac{529.5}{l_0}}} \quad \textbf{(5)}$$

where l is the current diameter at pressure p or temperature T; and l_0, is the initial diameter of the bubble at pressure p_0 or temperature T_0.

After the bubbles have been characterized, dynamic experiments have been performed and measured in the time domain. Interferometric fringes are detected by the photodetector when temperature or pressure vary and are recorded with the oscilloscope. The photodiode signal is steady with time at constant temperature and pressure, however, since the room temperature and pressure change slowly with time, the photodiode signal experiences a slow drift, this drift is smaller than the noise of the signal in intervals of time of several seconds and has no significant effect in the dynamic measurements we have carried out.

The liquid containing a microbubble was heated and its temperature raised without control. Interferometric fringes were measured with an oscilloscope in a time interval of 150 seconds, during this interval the temperature of the liquid increased in a range of [44.5±0.1^{0}C, 50.0±0.1^{0}C] at an average

rate 0.037 ^{0}C/s, the initial and the final temperatures were measured with a thermometer. The interference pattern measured in the 150 s window is shown in Fig. 8 (a), in this interval 179 fringes were recorded. Four temperature readouts have been obtained within each interferometric fringe (at maximum, minimum and inflection points), the diameter of the bubble increases one eighth of the wavelength (193.75 nm) between consecutive readouts, and equation (4) provides the corresponding increment of temperature. Fig. 8 (b) shows the temperature as function of the readout number, the plot shows as well the intervals of time between consecutive readouts, these intervals are comprised between 100 and 300 ms depending on the local velocity of variation of the bubble diameter. Using these data (T_0=45.0±0.1 ^{0}C and 179 fringes - or 716 readouts-) the calibration equation (4) predicts a final temperature of 50.1±0.1 ^{0}C which agrees with final reading of the thermometer (50.0±0.1 ^{0}C). The temporal evolution of temperature can be obtained from the lapses of time between readouts, the result is plotted in Fig. 8 (c), the line has a small curvature indicating a nonlinear variation of temperature during the heating process. Temperature has been readout in a minimum interval of 100ms as it can be seen in Fig. 8 (b), therefore the maximum sampling rate in the experiment has been 10 s^{-1}. The thermal sensitivity is given by the temperature variation between consecutive data points, the sensitivity is constant because the diameter is proportional to temperature, the resolution achieved in this demonstration has been 0.007 ^{0}C approximately, this resolution could be further improved by special electronics or algorithms capable of measuring smaller variations of the phase [20, 21]. The results are independent on the initial diameter of the bubble, just for completeness the bubble size was measured in the wavelength domain at time t=0 (temperature T_0=45.0±0.1 ^{0}C), the bubble had an initial diameter l_0= 120±3 µm and increased its size 138.7±0.2 µm up to a final diameter of 259±3 µm.

Notice that the key parameter to increase the temperature (or pressure) resolution is the interval of time that can be correlated with a variation of phase within an interferometric fringe (what we call the read out time), in our case this interval is ¼ of a fringe. The readout time determines the temporal resolution in a specific measurement and informs as well about the speed at which a parameter has been measured. We must point out that we have obtained the time intervals by software from the oscilloscope trace; alternatively, the number of interferometric fringes could have been directly captured by a commercial counter, but the resolution would have worsened by a factor of four unless the photodiode signal were electronically processed before counting in order to increase the number of phase correlated readouts per fringe.

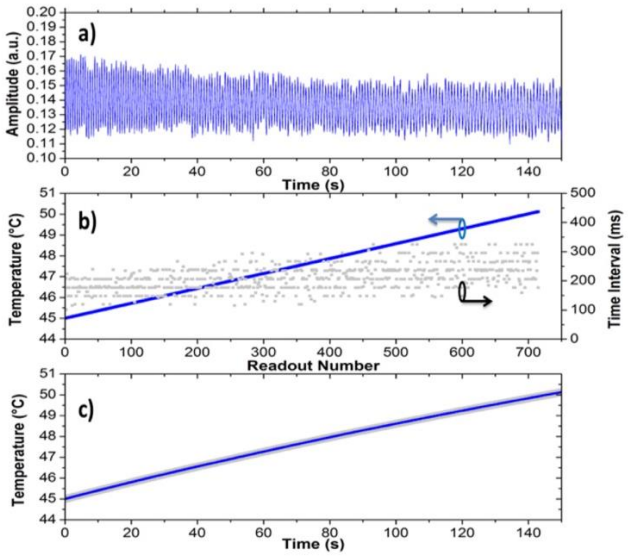

Figure 8. (a) Oscilloscope trace of the interferometric fringes when temperature varies. (b) Temperature readouts (line) obtained from Fig. 8-a, time intervals (dots) between consecutive readouts. (c) Temperature as function of time, the narrow grey area indicates the confidence range.

To demonstrate the full potential of the conic probe, the bubble was subjected to a pressure shock by opening suddenly the pressure regulator. The bubble had an initial diameter of 175 ±3 µm (measured in the wavelength domain) and pressure was risen from 1.1 to 3.5±0.1 bar. Fig. 9 (a) shows the interference fringes observed in the oscilloscope due to the compression of the bubble, the trace has been registered at a sampling rate of 10^5 s^{-1}, each interferometric fringe has a minimum of 20 sampling points. The trace shows that the pressure takes about 200 ms to reach a stationary, a no uniform fringe spacing can be clearly seen indicating a possible nonlinear evolution. In this figure, a total number of 97.5 fringes is observed, therefore, the final diameter of the bubble is 100±2 µm according to equation (2). From these data (p_0=1.1±0.1 bar, l_0=175±3 µm and 97.5 fringes) the calibration equation (5) predicts a final pressure in the bubble of p=3.4±0.1 bar, which is in reasonable agreement with the value obtained from the pressure gauge (3.5±0.1 bar). It is worth observing in Fig. 9 (a) that the photodetector signal is constant before the pressure shock when pressure and temperature were constant, this is a proof of the stability of the interferometer during short periods of time when environmental conditions does not change.

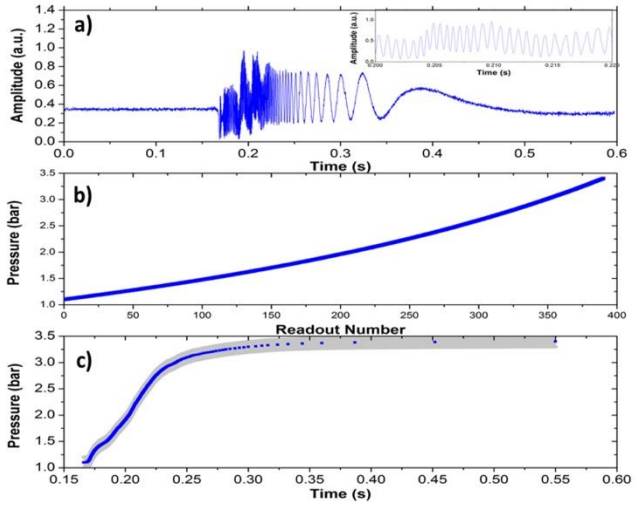

Figure 9. (a) Oscilloscope trace of the interferometric fringes during a shock of pressure, the inset shows a detail. (b) Pressure readouts obtained from Fig. 9-a. (c) Pressure as function of time (the grey area indicates the confidence range).

Fig. 9 (b) presents the pressure calculated from the interferometric fringes, four pressure readouts have been obtained from each single fringe, the nonlinear behavior of the plot is in agreement to the curvature of the calibration equation (5). Fig. 9 (c) presents the pressure as function of time, pressure rises in 81 ms to 90% of the final value at an average rate of 25 bar/s and tends asymptotically to the steady value in more than 150 ms.

In Fig. 10 we show the intervals of time within each pressure sample have been obtained, it can be observed that pressure has been readout in minimum time interval of 50 μs, therefore the maximum sampling rate of pressure has been 20000 s^{-1} (with at least 5 oscilloscope samples per each pressure readout); the scattering of the plotted dots are due to local variations of pressure that can be precisely detected by the system. This figure shows as well the variation of pressure detected in each readout point; we see that the smallest variation of pressure that has been detected in the full span of the pressure shock is 3.4 mbar.

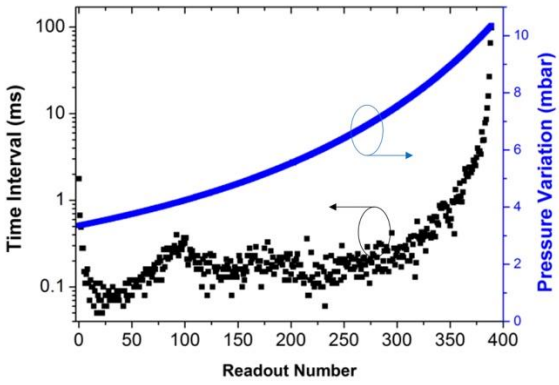

Figure 10. Pressure sampling intervals and pressure variations between consecutive pressure readouts.

4. Conclusions

In this article, we have presented the fabrication procedure and the performance of a conic optical fiber probe for photothermal generation and test of microbubbles in liquids. The bubbles are trapped by the cone which provides mechanical stability and prevents misalignment or detachment. It has been demonstrated that the conic probe can fasten large bubbles better than flat terminated probes, as a consequence the fiber diameters can be measured with improved accuracy and the bubbles are resistant to sudden environmental changes. Bubbles with diameters over 100μm have been used in the experiments due to their long lifetime (tens of minutes without pump power), the diameters of the bubbles have been interferometrically characterized as a function of temperature and pressure with an accuracy of 1.5%. Changes of pressure and temperature down to 0.007 ^{0}C and 3.4 mbar have been detected as a function of time at a maximum rate of 20000 readouts/s; small and fast variations can be detected, enabling the characterization of fast phenomena. The probe could be used in microfluidics to characterize the state of the fluid and the bubble itself, as well as for matter manipulation.

Funding

This work was supported by CONACyT grant number A1-S-28440 (Mexico), by the Ministerio de Ciencia e Innovación of Spain and Fondo Europeo de Desarrollo Regional (Ref.: PID2019-104276RB-I00), and by the Generalitat Valenciana of Spain (Ref.: PROMETEO-2019-048).

References

[1] O.V. Angelsky; A. Ya. Bekshaev; P.P. Maksimyak; A.P. Maksimyak; S.G. Hanson; S.M. Kontus, Controllable generation and manipulation of micro-bubbles in water with absorptive colloid particles by CW laser radiation, Opt. Express 25 (5) (2017) 5242-5243.

[2] J.G. Ortega-Mendoza, J.A. Sarabia-Alonso, P. Zaca-Moran, A. Padilla-Vivanco, C. Toxqui-Quitl, I. Rivas-Cambero and R. Ramos-Garcia, Marangoni force-driven manipulation of photothermally-induced microbubbles, Opt. Express 26 (6) (2018) 6653-6662.

[3] C. Hoera, M.M. Skadel, S.A. Pfeiffer, M. Pahl, Z. Shu, E. Beckert, D. Belder, A chip-integrated highly variable thermal flow rates sensor, Sens. Actuators B: Chem. 225 (2015) 42–49.

[4] R. Bue, A. Dudus, D. Uttamchandani, 2016; A review of single mode fibre fuidics, IEEE J. Selected Topics Quantum Electron. 22 (2) (2016) 9100112.

[5] L. Szekely, J. Reichert, R. Freitag, Non-invasive nano-flow sensor for application in micro-fluidicsystems, Sens. Actuators A :Phys. 113(1) (2004) 48–53.

[6] V. Lien, F. Vollmer, Microfluidic flow rate detection based on integrated optical fiber cantilever, Lab Chip 7(10) (2007) 1352–1356.

[7] W. Wenhua, L, Fang, Large-range liquid level sensor based on an optical fibre extrinsic Fabry–Perot interferometer, Opt. Lasers Eng. 52, (2014) 201-205.

[8] T. Bae, R. Atkins, H. Taylor, W. Gibler, Interferometric fiber-optic sensor embedded in a spark plug for in-cylinder pressure measurement in engines, Appl. Opt. 42 (6) (2003) 1003-1007.

[9] Zhou, Y.; Seshia, A.A.; and Hall, E.A.H.; "Microfluidics-based Acoustic Microbubble Biosensor", 12th IEEE Sensors Conference Baltimore, MD, 2013, pp. 1-4, doi: 10.1109/ICSENS.2013.6688408.

[10] W. Xu, L. L. Wu, Y. Zhang, H. Xue, G.P. Li, M. Bachman, A vapor based microfluidic flow regulator, Sens. Actuators B Chem. 142(1) (2009) 355–361.

[11] J. Ma, G. Wang, L. Jin, K. Oh, A. P. Maksimyak, B. O. Guan, Photothermally generated bubble on fiber (BoF) for precise sensing and control of liquid flow along a microfluidic channel, Opt. Express 27 (14) (2019) 19786-19777.

[12] V. Kotaidis, C. Dahmen, G. Plessen, F. Springer, A. Plech, Excitation of nanoscale vapor bubbles at the surface of gold nanoparticles in water, J. Chem. Phys. 124, (2006) 184702.

[13] C. L. Zhang, Y. Gong, W.L. Zou, Y. Wu, Y.J. Rao, G.D. Peng, X. Fan, Microbubble-Based Fiber Optofluidic Interferometer for Sensing, J. Lightwave Technol. 35 (13) (2017) 2514-2519.

[14] J.G. Ortega-Mendoza, F. Chavez, P. Zaca-Moran, F.C. Mendoza, G.F. Perez-Sanchez, G. Beltran-Perez, R. Ramos-Garcia, Selective photodeposition of zinc nanoparticles on the core of a single-mode optical fiber, Opt. Express 21, (5) (2013) 6509-6518.

[15] P. Zaca-Moran, R. Ramos-Garcia, J.G. Ortega-Mendoza, F. Chavez, G.F. Perez-Sanchez, F.C. Mendoza, Saturable and two-photon absorption in zinc nanoparticles photodeposited onto the core of an optical fiber, Opt. Express 23, (14) (2015) 18721-18729.

[16] M. Marrese, H. Offerhaus, E. Paardekan, D. Iunnuzzi, 70 μm diameter optical probe for common-path optical coherence tomography in air and liquids, Opt. Lett. 43 (24) (2018) 5929-5932;

[17] M. Getzlaff, M. Leifels, P. Weber, Ü. Kökcam-Demir , Ch. Janiak, Nanoparticles in toner material, SN Appl. Sci. 1 (2019) 489. https://doi.org/10.1007/s42452-019-0501-9

[18] R.S. Taylor, C. Hnatovsky, Growth and decay dynamics of a stable microbubble produced at the end of a near-field scanning optical microscopy fiber probe, J. Applied Phys. 95 (12) (2004) 8444-8449.

[19] Dortmund Data Bank 2020, http://www.ddbst.com/en/EED/PCP/SFT_C174.php

[20] J. Xie, F. Wang F, Y. Pan, J. Wang, Z. Hu, Y. Hu, High resolution signal-processing method for extrinsic Fabry–Perot interferometric sensors, Opt. Fiber Technol. 22, (2015) 1–6

[21] D. Tosi, S. Poeggel, G. Leen, E Lewis, Adaptive filter based interrogation of high-sensitivity fiber optic FabryPerot interferometry sensors, Sens. Act. A: Phys; 206, (2014) 144-150.